ARTICLES

Charge Carrier Dynamics in Metalated Polymers Investigated by Optical-Pump Terahertz-Probe Spectroscopy

Paul D. Cunningham,*,† L. Michael Hayden,† Hin-Lap Yip,‡ and Alex K.-Y. Jen‡

Department of Physics, University of Maryland Baltimore County, Baltimore, Maryland 21250, Department of Materials Science and Engineering, University of Washington, Seattle, Washington 98195-2120

Received: July 8, 2009; Revised Manuscript Received: October 9, 2009

We report charge carrier dynamics in solid films of a series of metalated polymers based on Pt- and 4,7-di-2′-thienyl-2,1,3,-benzothiadiazole or 4,7-di-2′-thienothienyl-2,1,3,-benzothiadiazole upon photoexcitation of the $\pi-\pi^*$ transition using optical-pump terahertz-probe spectroscopy. Subpicosecond generated charge carriers recombine within 100 ps, but bound excitons persist. Application of the Drude−Smith model allows for estimation of the intrinsic mobility and internal quantum yield of charge carrier generation in these films. Thermal annealing is found to have no effect on nanometer scale charge transport.

Introduction

Semiconducting π-conjugated polymers are under intense study for potential applications in electronic devices; for example, organic field-effect transistors (OFET) and organic photovoltaics (OPV). Much attention has been given to material systems with strong $\pi-\pi$ interactions that self-assemble into polycrystalline films; for example, poly(3-hexylthiophene-2,5-diyl) (P3HT).[1] Although these systems exhibit high OFET mobilities[2] and OPV power conversion efficiencies (PCE),[3] their optoelectronic properties are highly sensitive to processing conditions.[4,5]

Alternatively, amorphous films with properties insensitive to processing conditions are desirable. However, OFET mobilities in amorphous systems are typically much lower than those in organic crystalline systems, which are known to exhibit bandlike transport.[6] Additionally, there is a desire for narrow-band-gap systems to improve light-harvesting in OPVs.[3,7] Recent theoretical studies predict that achieving OPV PCE >10% is possible only by reducing the donor material bandgap to <1.74 eV (713 nm),[8] although other models argue that larger bandgaps (1.9 eV) are necessary.[9] However, the PCE of OPVs based on narrow gap films have typically been limited to 3.5%[10] unless additives are used, in which case a PCE of 5.5% was reached.[11] Very recently, optimization of the blend ratio, choice of solvent, and addition of a TiO_x spacer layer has led to a PCE of 6.1%, the highest reported to date, in an OPV cell based on a narrow-bandgap donor.[12]

A less explored option for improved solar spectrum coverage and favorable charge transport properties involves the use of metalated polymers. The inclusion of platinum (Pt) has been shown to improve donor strength in push−pull polymers by enhancing the delocalization through overlap of the d orbitals of the metal with the π orbitals of the aromatic.[13] When combined with a strong electron acceptor, this leads to a charge-transfer complex with absorption approaching the infrared (IR).[14] In some systems, the addition of Pt has been shown to increase rapid intersystem crossing through the heavy atom effect,[15] allowing for the long-lived triplet state to participate in electron transfer in OPVs.[16] A review of research in this area is given by Wong, et al.[17] OPVs based on Pt and 4,7-di-2′-thienyl-2,1,3,-benzothiadiazole (DTBTD) have achieved PCEs as high as 4.93% without the use of additives or postprocessing steps.[14] Although these PCE values have come under scrutiny,[18,19] this material system represents an alternative avenue from the popular P3HT/[6,6]-phenyl-C_{61}-butyric acid methyl ester (PCBM) system to achieving efficient OPV cells. Recently, it has been shown that the hole mobility can be improved by substituting thieno[3,2-*b*]thiophene (TT) for the thiophene (T) donor,[13] resulting in improved OFET performance and enhanced OPV PCEs.

Optical-pump terahertz-probe (OPTP) spectroscopy, that is, time-resolved terahertz (THz) spectroscopy, has become a powerful all-optical, noncontact tool for investigating local charge transport and ultrafast charge carrier generation with subpicosecond resolution.[20,21] It is a technique that is analogous to photoinduced absorption spectroscopy but is performed in the far-IR part of the electromagnetic spectrum with a nonperturbing low energy (<10 meV) photon probe. Because typical carrier scattering times are between 10 fs and 1 ps with corresponding scattering rates in the frequency range 1−100 THz, the THz probe is directly sensitive to charge carriers. Because coherent detection methods are commonly employed, the frequency-dependent complex dielectric properties are accessible, allowing for the distinction between tightly bound excitons[22] and free carriers.[23] Due to its high frequency, as compared to direct current (DC) measurements, THz radiation probes charge transport over nanometer length scales as defined by $L_\omega = \sqrt{(D/\omega)}$, where D is the Einstein diffusion constant given by $D = \mu k_b T/e$, where μ is the mobility, e is the fundamental charge, and k_bT is the thermal energy.[24] Recently, we have shown that OPTP can be used to extract the intrinsic mobility[25] from P3HT,[26] which is known to self-assemble into

* Corresponding author. E-mail: pcunni1@umbc.edu.
† University of Maryland Baltimore County.
‡ University of Washington.

10.1021/jp906454g CCC: $40.75
Published on Web 11/03/2009

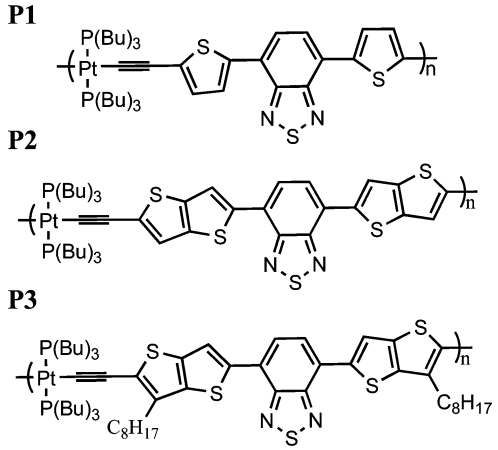

Figure 1. The chemical structures of Pt-polymers P1, P2, and P3.

a polycrystalline film with grains larger than L_ω.[1] This is in contrast to the mobilities measured in devices that are disorder-limited, measured over micrometer-scale distances, subject to defects and conjugation breaks, and influenced by extrinsic factors, such as electric fields and electrode work functions.[27] Here, we compare the ultrafast dynamics and local transport properties of Pt-polymers based on DTBTD and 4,7-di-2′-thienothienyl-2,1,3,-benzothiadiazole (DTTBTD) to these same quantities in P3HT. We also explore the effects of annealing on nanoscale charge transport.

Experimental Methods

The metalated polymers P1, P2, and P3 (Figure 1) were synthesized following the procedures of Baek et al., with molecular weights of 1.49, 1.1, and 1.86 × 10^4 g/mol.[13] Solid films of P1−3 were prepared from solution. Quick drying solvents (e.g. chloroform) produce brittle films of P2 and P3 owing to the more rigid structure of the fused TT, necessitating slow solvent removal. All films for OPTP were drop-cast from 20 mg/mL chlorobenzene solutions onto GE-124 fused-silica substrates kept on a 60 °C hot plate. Whereas films of P2 would become brittle over time, the addition of alkyl chains to the TT leads to improved film quality for P3.

We performed linear ultraviolet and visible absorption spectroscopy on 1000 rpm spin-coated films on fused-silica substrates using a Perkin-Elmer Lambda 3B spectrophotometer. The absorption coefficient was found from the absorbance spectra using $\alpha = \mathrm{OD}\ \ln(10)/z$, where z is the film thickness and OD is the measured optical density. Film thicknesses were determined using a KLA Tencor Alpha-Step IQ surface profilometer.

A detailed description of our OPTP experimental setup and its operation can be found elsewhere.[26] The fundamental laser source for THz generation, detection, and optical excitation is a 900 μJ, 1 kHz repetition rate, 45 fs, Ti:sapphire laser (Spectra-Physics, Spitfire). We use a 100 mm BK7 lens to focus 350 μJ through a 100 μm, type II, β-barium borate (BBO) crystal to form a filament for air plasma THz generation via mixing of the fundamental and second harmonics.[28−31] Residual UV, visible, and IR are blocked using a 400 μm high-resistivity silicon wafer at Brewster's angle. The THz beam is focused to about 0.8 mm at the sample position. A small part of the fundamental, 900 nJ, is focused onto the 2 mm (110) ZnTe detector crystal, where collinear propagation with the THz beam is achieved using an IR coated pellicle. We obtain the 400 nm pump beam by frequency-doubling the 800 nm fundamental in a 300 μm thick, type I BBO crystal and subsequently focus this beam to a 2.3 mm diameter spot at the sample. The beam spot size, d_0, was determined by measuring the transmission, P, through a pinhole of known size, d_{PH}, and relating it to the incident power, P_0, via $P = P_0(1 - e^{-2d_{PH}^2/d_0^2})$.

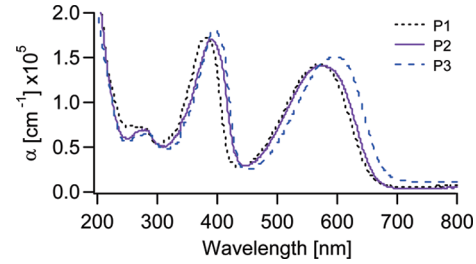

Figure 2. UV/visible absorption spectra of P1, P2, and P3. The visible absorption feature is due to the charge transfer complex, whereas the UV absorption is associated with the $\pi-\pi^*$ transition.

The pump-induced modulation of the transmitted THz field was monitored as a function of delay with respect to photoexcitation. Because the entire THz bandwidth is in phase at the time-domain waveform peak, changes in peak transmission yield the average excited-state dynamics in what is known as a pump scan. When very little phase shift is present, $\Delta E/E_0(t, \tau)$ is proportional to the product of the mobility, $\mu(\tau)$, and carrier density, $N(\tau)$, where t is the time domain variable and τ is the delay with respect to optical excitation. For probe scans, the differential transmission of the complete THz waveform through the excited sample is recorded. Through Fourier analysis, the frequency-dependent complex conductivity is obtained. The frequency response can be modeled allowing for the determination of the carrier density and mobility. Following the work of Nienhuys and Sundstrom,[32] we use the following model of THz transmission through a thin photoexcited sample:

$$\tilde{\sigma}(\omega, \tau) = -\frac{n_{\mathrm{THz}} + n_{\mathrm{air}}}{Z_0 d}\frac{\Delta\tilde{E}(\omega, \tau)}{\tilde{E}_0(\omega)} \qquad (1)$$

where Z_0 is the impedance of free space; d is the $(1/e)$ absorption depth of the pump beam; and n_{THz} and n_{air} are the THz indices of refraction of the unexcited sample and air, respectively. For most polymers, there is little absorption, and we can take the THz index of refraction to be frequency-independent. The THz indices (n_{THz}) of P1−3 were measured to be 1.9 using time-domain spectroscopy.

Results/Discussion

Linear absorption spectra of solid films of P1−3 are shown in Figure 2. The absorption features in the UV are attributed to the $\pi-\pi^*$ transition, and those in the visible, to the charge-transfer complex,[14] reducing the bandgap to ∼1.8 eV. The lack of higher-order structure in the spectra and their similarity to published spectra in solution indicates a lack of long-range order in these polymer films, consistent with X-ray diffraction studies.[13] The red-shifted absorption of P3 with respect to P2 and P1 is caused by increased delocalization as the additional alkyl chains strengthen the donor. We do not see a significant redshift from P1 to P2, which is surprising because the reduced delocalization in the fused-ring TT lowers the highest occupied molecular orbital (HOMO) energy of poly(2,5-bis(3-alkylthiophen-2-yl)thieno[3,2-*b*]thiophene (PBTTT) as compared to P3HT.[33] We measured the absorption depths at the 400 nm pump

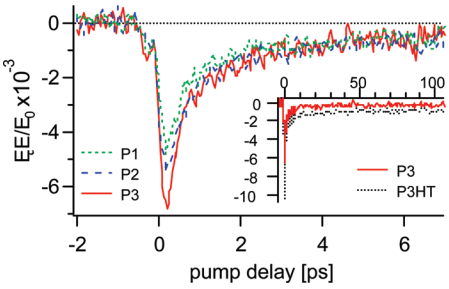

Figure 3. Comparison of conductivity dynamics in Pt-polymers for 400 nm excitation at a fluence of $2.0 \pm 0.2 \times 10^{19}$ photons/m^2. Inset: Comparison of conductivity dynamics in P3 to P3HT.

wavelength to be 75 ± 6, 62 ± 5, and 56 ± 5 nm for P1, P2, and P3 respectively.

All films were photoexcited with 46 mW of 400 nm light, equivalent to a fluence of 2×10^{19} photons/m^2. The resulting dynamics from excitation above the $\pi-\pi^*$ transition in P1−3 are similar to those seen for P3HT,[26] a fast ~1 ps decay followed by a long-lived state that persists for >100 ps (Figure 3 inset). Comparison of the pump scan dynamics of P1−3 shows an increase in the initial photoresponse upon replacing the T donor (P1) with the fused TT (P2) (Figure 3). This is consistent with previous reports of TT improving local order, increasing the conjugation length, and the probability of charge transfer, as compared to T.[34] The further increase in conductivity seen in P3 is consistent with device measurements and may be related to the increased delocalization of the donor caused by the additional alkyl groups.[13]

To compare dynamics in materials, typically, one compares the conductivity instead of the normalized change in THz transmission, but even at constant fluence, differences in the absorption depths lead to different maximum carrier densities achievable in the film and, thus, different conductivities. We can utilize the following time domain relationship,[35] which holds for small changes in transmission,

$$\tilde{\sigma}(\tau) = -\frac{2n_{\mathrm{THz}}}{Z_0 d}\frac{\Delta\tilde{E}(t_{\max},\tau)}{\tilde{E}_0(t_{\max})} \qquad (2)$$

where $t_{\max}$ corresponds to the time-domain position of the peak THz transmission. We recall that the conductivity is proportional to the mobility and carrier density. We can also relate the carrier density to the number of absorbed photons, N_0, and thus the fluence, F, via

$$N = \phi N_0 = \phi\frac{F}{d}T(1 - \mathrm{e}^{-\alpha z}) \qquad (3)$$

where z is the film thickness, α is the absorption coefficient at the pump wavelength, ϕ is the photon-to-carrier yield (i.e. the internal quantum efficiency (IQE)), and T is the Fresnel transmission coefficient. For samples sufficiently thick to absorb nearly all of the nonreflected light (e.g. a thickness of $4.6d$ provides 99% pump beam absorption based on the Beer−Lambert law), we arrive at

$$-\frac{\Delta E}{E} \propto \frac{Z_0 TF\phi\mu}{2n_{\mathrm{THz}}} \qquad (4)$$

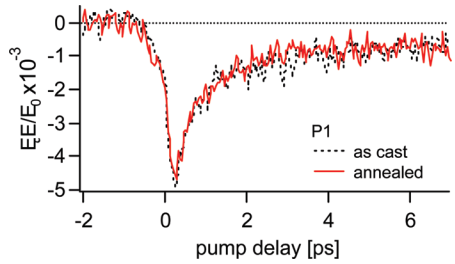

Figure 4. A comparison of conductivity dynamics in an as-cast film of P1 to a thermally annealed film of P1 shows no change.

So for materials with similar optical and THz indices, a comparison of pump scans at constant fluence is proportional to the product of the mobility and the carrier yield, which is the case for P1−3. In the case that the indices of refraction are different, it is a simple matter to scale the pump scans for a straightforward comparison. For example, given optical and THz indices of 1.96[14] and 2.22,[36] respectively, the pump scan of P3HT in the inset of Figure 3 was increased by 15% for a fair comparison to P1−3. It bears mentioning that we should not utilize the relationship $\sigma = ne\mu$, which holds only for the DC conductivity. However, this relationship has successfully been used in the past to describe organic crystals,[37] which, unlike polymers that exhibit dispersive transport, show frequency-independent conductivity.

Postprocessing techniques (e.g. thermal annealing) have been shown to improve the long-range order and enhance the hole mobility in P3HT[38] as well as the OPV PCE in P3HT/PCBM bulk heterojunction cells.[5] Annealing films of P1−3 at 150 °C for 10 min in vacuum showed no change in the conductivity dynamics (Figure 4), which is consistent with measurements made on OPVs.[13]

The frequency dependence of the complex conductivity observed in P1−3 at early time delays (Figure 5) is similar to that seen in P3HT,[26] which is characteristic of inhibited long-range transport.[22] Polymer systems can contain random defects that cause destructive interference among scattering events and slow the ensemble motion of carrier propagation through an effect called Anderson localization.[39] This type of carrier localization can be described by the Drude−Smith model (DSM),[40]

$$\tilde{\sigma}(\omega) = \frac{\varepsilon_0\omega_{\mathrm{p}}{}^2\tau}{1 - i\tau\omega}\left(1 + \sum_{n=1}^{\infty}\frac{c_n}{(1 - i\tau\omega)^n}\right) \qquad (5)$$

where $\omega_{\mathrm{p}}{}^2$ is the plasma frequency, τ is the scattering time, ε_0 is the permittivity of free space, and c is the persistence of velocity of each scattering event. Typically, the series is truncated to contain only the first scattering event such that the first scattering event is ballistic and all subsequent events are diffusive. The persistence of velocity is allowed to assume values $-1 \le c \le 0$ to describe varying degrees of backscattering or carrier localization. The DSM has been successfully applied to the THz conductivity of dye-sensitized solar cells,[41] nanocrystalline silicon,[42] BHJ OPV cells,[36] and the percolative insulator−metal transition in thin gold films.[43] We separate eq 5 into its real and imaginary parts and fit it simultaneously to the real and imaginary parts of $\tilde{\sigma}(\omega)$, yielding the scattering time, plasma frequency, and persistence of velocity. If we neglect the carrier density dependence of the hole mobility over the range of carrier densities achieved here, we can assume that the hole mobility is the same for all delays for a given material,

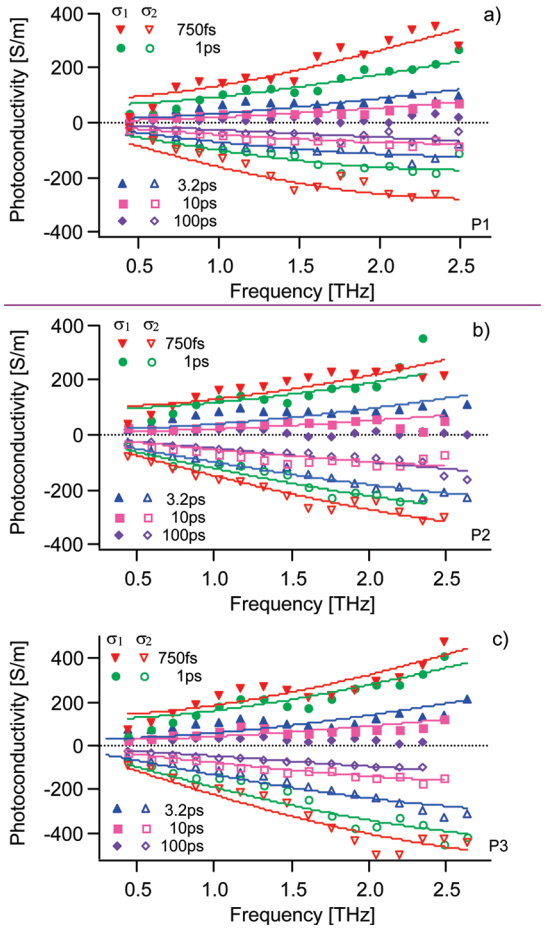

Figure 5. The extracted frequency-dependent real (solid) and imaginary (open) conductivity of (a) P1, (b) P2, and (c) P3 measured at 750 fs (upside down triangle), 1 ps (circle), 3.2 ps (triangle), 10 ps (square), and 100 ps (diamond) after photoexcitation. The solid lines for all but 100 ps delay are best fits to the DSM. The solid line for 100 ps is a best fit to the Lorentz−Oscillator model for a bound exciton.

which is consistent with previous observations in other material systems.[36] Therefore, the scattering time is kept as a global variable for all delays, and its value represents the best fit for all conductivity curves for a given material. The mobility can be calculated from the scattering time using $\mu = e\tau/m^*$, and the carrier density, from $N = \varepsilon_0\omega_p^2 m^*/e^2$, where m^* is the effective carrier mass. For the purpose of estimating the mobility and carrier yields, we have assumed that the effective hole mass in these polymers is the same as P3HT,[25] 1.7× the mass of an electron. Given the fluence and absorption depth, we can estimate the IQE from eq 3 as $\phi(\lambda) = N_0 T(\lambda)\mathrm{d}(\lambda)/F$ at the pump wavelength, where $T(\lambda)$ is the Fresnel transmission coefficient based on an optical index of refraction of 2.04.[14] An estimate of the DC mobility is given by $\mu_{DC} = \mu(1 + c_1)$.

The hole mobility and carrier yields found using the DSM are summarized in Table 1. We do not see an increase in mobility upon replacing T in P1 with TT (P2) but, instead, an increase in the quantum yield. This is inconsistent with the order of magnitude increase in field-effect mobility from OFET measurements.[13] It is possible that the change transport properties over macroscopic distances, as measured in OFET devices, differs greatly as compared to the transport over nanometer scale distances measured here. For example, the OFET mobility[2] of P3HT agrees with time-resolved microwave conductivity measurements[44] because they probe charge transport over similar length scales but are orders of magnitude smaller than the intrinsic mobility[25] and values determined by THz studies.[26,36] Device measurements are also influenced by extrinsic factors, such as applied fields and the electrode work function.[27] P2 may exhibit better long-range transport than P1, which is consistent with reports that TT improves long-range order as compared to T.[34] Our extracted mobilities are consistent with theoretical calculations predicting a reduced intrinsic mobility in crystalline PBTTT as compared to P3HT.[25] Previous THz studies showed a large improvement in the conductivity in PBTTT as compared to P3HT[34] with a similar trend as seen in OFET devices;[45] however, these conclusions were based on the pump-scan dynamics only, and similar carrier yields were assumed. We see similar hole mobilities in P3 and P2, as one might expect from the similar chemical structure. The improved OPV PCE seen in P3 as compared to P2, given the similar μ, ϕ, HOMO, and lowest-unoccupied molecular orbital values, reflects a device mobility improvement that is likely morphological in origin. The monotonically decreasing c values indicate the charge carriers are becoming more localized with increasing delay.

At long delays (i.e. 100 ps), the DSM can no longer describe the complex conductivity of these materials (Figure 6). The real conductivity becomes suppressed while a negative linear imaginary conductivity persists. This is the signature of a tightly bound exciton,[22] which can be described by a Lorentz oscillator with a center frequency, representing the exciton binding energy, much larger than the experimentally available frequency range of 0.3−2.5 THz (1.2−10 meV). In such a case, the Lorentz oscillator model simplifies to

$$\tilde{\sigma}(\omega) = -i\varepsilon_0\omega\Delta\varepsilon \qquad (6)$$

where $\Delta\varepsilon$ is change in the dielectric constant associated with the polarizability of bound excitons. This is different from the frequency-dependent conductivity observed at long delays in P3HT, where a DSM-like trend persists for >150 ps.[46] As P3HT self-organizes into a polycrystalline lamellar structure, there is a much larger degree of local order than seen in amorphous polymers. The improved interchain transport in that material system may be responsible for the more efficient charge carrier generation. Without this intrinsic exciton separation mechanism, amorphous polymers (e.g. PPV[22]) show excitonic characteristics at long time delays. Electric fields and charge-separating interfaces present in device geometries allow charge carriers to persist in OPVs and OFETs.

It is possible to estimate the polarizability, α, of the exciton from the change in the dielectric constant using the Clausius−Mossotti relation

$$\frac{n_{THz}^2 - 1}{n_{THz}^2 + 2} + \frac{\alpha\phi_{exc}N_0}{3} = \frac{n_{THz}^2 - 1 + \Delta\varepsilon}{n_{THz}^2 + 2 + \Delta\varepsilon} \qquad (7)$$

where ϕ_{exc} is the IQE of exciton generation, assuming an IQE of 1 yields 350 ± 70, 700 ± 100, and 800 ± 100 Å^3 for the lower limit of the exciton polarizability in P1, P2, and P3, respectively. We can estimate the upper limit of the exciton binding energy from the lower limit of the exciton polarizability, because the two are inversely related. The values shown here imply that the upper limit of the exciton binding energy is greater than 1 eV for P1 and between 0.8 and 1 eV for P2 and P3.[47] The polarizability may be much larger because the singlet exciton fluorescence quantum efficiency is low,[19] and thus, the IQE of exciton generation may be significantly less than 1.

TABLE 1: Results of DSM Fits to the Frequency-Dependent Complex Conductivity Found in Figure 5

delay (ps)	τ (fs)	ω_p (THz)	c	$\Delta\varepsilon$	N (10^{23} m^{-3})	ϕ (%)	μ (cm^2/(V s))	μ_{dc} (cm^2/(V s))
				P1 $N_{max} = 27 \pm 3 \times 10^{25}$ m^{-3}				
0.75	24 ± 1	79 ± 4	−0.937		34 ± 3	1.3 ± 0.2	25 ± 1	1.6 ± 0.2
1	24 ± 1	63 ± 3	−0.928		21 ± 2	0.8 ± 0.1	25 ± 1	1.8 ± 0.2
3.2	24 ± 1	50 ± 3	−0.98		14 ± 2	0.51 ± 0.09	25 ± 1	0.5 ± 0.2
10	24 ± 1	39 ± 3	−0.98		8 ± 1	0.31 ± 0.06	25 ± 1	0.5 ± 0.5
100				0.48 ± 0.07				
				P2 $N_{max} = 32 \pm 4 \times 10^{25}$ m^{-3}				
0.75	16 ± 1	111 ± 8	−0.943		70 ± 10	2.1 ± 0.4	17 ± 1	0.94 ± 0.09
1	16 ± 1	101 ± 8	−0.936		55 ± 9	1.7 ± 0.3	17 ± 1	1.1 ± 0.1
3.2	16 ± 1	87 ± 7	−0.982		41 ± 7	1.3 ± 0.3	17 ± 1	0.3 ± 0.1
10	16 ± 1	63 ± 5	−0.98		21 ± 3	0.7 ± 0.1	17 ± 1	0.3 ± 0.2
100				0.89 ± 0.07				
				P3 $N_{max} = 35 \pm 4 \times 10^{25}$ m^{-3}				
0.75	17 ± 1	125 ± 7	−0.945		84 ± 9	2.4 ± 0.4	18 ± 1	1.00 ± 0.09
1	17 ± 1	116 ± 7	−0.943		73 ± 9	2.1 ± 0.4	18 ± 1	1.0 ± 0.1
3.2	17 ± 1	93 ± 6	−0.978		47 ± 6	1.3 ± 0.2	18 ± 1	0.4 ± 0.1
10	17 ± 1	72 ± 5	−0.97		28 ± 4	0.8 ± 0.1	18 ± 1	0.5 ± 0.2
100				0.8 ± 0.1				

Given the relatively low yield of free carriers, it is likely that excitons are the primary photogenerated product and that the charge carriers present at early delays are the result of hot exciton dissociation. The pump beam possesses 1.2 eV of excess energy over the bandgap, which here refers to the onset of linear absorption due to the charge transfer complex, which would be more than sufficient to separate a significant fraction of excitons into charge carriers. These charge carriers rapidly decay as they thermalize, no longer processing sufficient energy to escape defects in the polymer chain or to tunnel to adjacent chains, which is consistent with the increased localization at long delays. However, the low fluorescence quantum yield[18,19] points to a low density of excitons persisting at 100 ps after photoexcitation. This leads to a higher estimated exciton polarizability. If a large number of highly polarizable excitons were created at early delays, we would expect to see some noticeable contribution from them to the complex conductivity, given the estimated lower limit of the exciton polarizability.

Instead, the conductivity at early delays is dominated by dispersive transport of charge carriers, and addition of an excitonic term to the DSM fits, as previously done in studies of P3HT at long delays,[36] shows no dependence on $\Delta\varepsilon$ and yields no improvement. Clearly, the response of dispersive carrier transport masks any excitonic response that might be present at early delays, as was the case in previous studies of P3HT at early delays.[36] Given the similar dynamics and excitonic response seen in PPV,[22] we do not believe impurity trapping played a role in the results seen here. It is not clear what role intersystem crossing to the triplet state plays in the observed dynamics, because low phosphorescence yields[17] and microsecond-scale, long-lived metastable excited states have previously been observed,[19] placing the branching ratio under debate. To confirm the supposition that excitons are the primary photoproduct, photoconductivity experiments should be performed to ascertain whether the onset of photoconduction is coincident with the onset of absorption. If higher-energy photons are needed to produce macroscopically mobile charge carriers, this is a clear indicator that the molecular exciton model applies and that excitons are the primary photogenerated species.

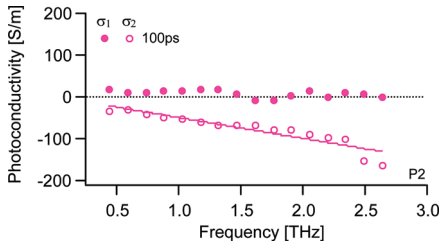

Figure 6. Frequency-dependent complex conductivity of P2 at a delay of 100 ps after photoexcitation, where the solid line is a fit to the Lorentz oscillator model for a bound exciton.

THz studies comparing conductivity dynamics resulting from the $\pi-\pi^*$ transition to those resulting from exciting the charge-transfer complex would also be useful in determining whether the excess excitation energy is responsible for charge carrier generation. They may also explain the lack of an excitonic signature at long delays in the narrow-gap polymer APFO-3 observed when optically exciting the charge transfer complex,[48] which may be due to more efficient separation of electrons and holes. Broadband THz studies, achievable through the use of polymer emitters and sensors[49] or ionized air plasmas,[50] would also aid in more precisely determining the scattering time and plasma frequency because, for the scattering rates seen in polymers, the DSM conductivity has distinct features outside of the currently available frequency band. Broadband OPTP studies would also allow for better comparison between different proposed conductivity models (e.g. DSM and the Lorentz oscillator model), which can reproduce the same trends at low frequencies (0−3 THz) but diverge at higher frequencies (>5 THz).

Summary

We performed OPTP spectroscopy on three metalated polymers and found that all three show signs of subpicosecond charge carrier generation. These charge carriers experience dispersive transport and decay over ∼100 ps, leaving behind bound excitons. This is in sharp contrast to the dynamics seen in P3HT, where charge carriers persist at long delays. The improved conductivity in P3 as compared to P1 is attributed to larger carrier yields. Thermal annealing is found to have no effect on nanometer scale charge transport. Future, broad bandwidth (0 − 10 THz) THz studies may provide further insight, allowing more accurate determination of material constants through the identification of resonant spectral features and clear discrimination among different conductivity models.

Acknowledgment. This material is based upon work supported by the STC program of the National Science Foundation No. DMR 0120967.

References and Notes

(1) Sirringhaus, H.; Brown, P. J.; Friend, R. H.; Nielsen, M. M.; Bechgaard, K.; Langeveld-Voss, B. M. W.; Spiering, A. J. H.; Janssen, R. A. J.; Meijer, E. W.; Herwig, P.; de Leeuw, D. M. *Nature* **1999**, *401*, 685.

(2) Wang, G.; Swensen, J.; Moses, D.; Heeger, A. J. *J. Appl. Phys.* **2003**, *93*, 6137.

(3) Kim, J. Y.; Lee, K.; Coates, N. E.; Moses, D.; Nguyen, T.-Q.; Dante, M.; Heeger, A. J. *Science* **2007**, *137*, 222.

(4) Li, G.; Shrotriya, V.; Huang, J.; Yao, Y.; Moriarty, T.; Emery, K.; Yang, Y. *Nat. Mater.* **2005**, *4*, 864.

(5) Kim, Y.; Choulis, S. A.; Nelson, J.; Bradley, D. D. C.; Cook, S.; Durrant, J. R. *Appl. Phys. Lett.* **2005**, *86*, 063502.

(6) Hegmann, F. A.; Tykwinski, R. R.; Lui, K. P. H.; Bullock, J. E.; Anthony, J. E. *Phys. Rev. Lett.* **2002**, *89*, 227403.

(7) Svensson, M.; Zhang, F.; Veenstra, S. C.; Verhees, W. J. H.; Hummelen, J. C.; Kroon, J. M.; Inganas, O.; Anderson, M. R. *Adv. Mater.* **2003**, *15*, 988.

(8) Scharber, M. C.; Muhlbacher, D.; Koppe, M.; Denk, P.; Waldauf, C.; Heeger, A. J.; Brabec, C. J. *Adv. Mater.* **2006**, *18*, 789.

(9) Koster, L. J. A.; Mihailetchi, V. D.; Blom, P. W. M. *Appl. Phys. Lett.* **2006**, *88*, 093511.

(10) Zhu, Z.; Waller, D.; Gaudiana, R.; Morana, M.; Mühlbacher, D.; Scharber, M.; Brabec, C. *Macromolecules* **2007**, *40*, 1981.

(11) Peet, J.; Kim, J. Y.; Coates, N. E.; Ma, W. L.; Moses, D.; Heeger, A. J.; Bazan, G. C. *Nat. Mater.* **2007**, *6*, 497.

(12) Park, S. H.; Roy, A.; Beaupre, S.; Cho, S.; Coates, N.; Moon, J. S.; Moses, D.; Leclerc, M.; Kwanghee, L.; Heeger, A. J. *Nat. Photon.* **2009**, *3*, 297.

(13) Baek, N. S.; Hau, S. K.; Yip, H. L.; Acton, O.; Chen, K. S.; Jen, A. K. Y. *Chem. Mater.* **2008**, *20*, 5734.

(14) Wong, W.-Y.; Wang, X.-Z.; He, Z.; Djurisic, A. B.; Yip, C.-T.; Cheung, K.-Y.; Wang, H.; Mak, C. S. K.; Chan, W.-K. *Nat. Mater.* **2007**, *6*, 521.

(15) Chawdhury, N.; Kohler, A.; Friend, R. H.; Younus, M.; Long, N. J.; Raithby, P. R.; Lewis, J. *Macromolecules* **1998**, *31*, 722.

(16) Guo, F.; Kim, Y.-G.; Reynolds, J. R.; Schanze, K. S. *Chem. Commun.* **2006**, *2006*, 1887.

(17) Wong, W.-Y. *Macromol. Chem. Phys.* **2008**, *209*, 14.

(18) Gilot, J.; Wienk, M.; Janssen, R. A. J. *Nat. Mater.* **2007**, *6*, 704.

(19) Mei, J.; Ogawa, K.; Kim, Y.-G.; Heston, N. C.; Arenas, D. J.; Zahra, N.; McCarley, T. D.; Tanner, D. B.; Reynolds, J. R.; Schanze, K. S. *Appl. Mater. Interfaces* **2009**, *1*.

(20) Beard, M. C.; Turner, G. M.; Schmuttenmaer, C. A. *J. Phys. Chem. B* **2002**, *106*, 7146.

(21) Hegmann, F. A.; Ostroverkhova, O.; Cooke, D. G. Probing Organic Semiconductors with Terahertz Pulses. In *Photophysics of Molecular Materials*; Lanzani, G., Ed.; Wiley-VCH: Weinheim, 2006.

(22) Hendry, E.; Schins, J. M.; Candeias, L. P.; Siebbeles, L. D. A.; Bonn, M. *Phys. Rev. Lett.* **2004**, *92*, 196601.

(23) Beard, M. C.; Turner, G. M.; Schmuttenmaer, C. A. *Phys. Rev. B* **2000**, *62*, 15764.

(24) Henning, P. F.; Homes, C. C.; Maslov, S.; Carr, G. L.; Basov, D. N.; Nikolic, B.; Strongin, M. *Phys. Rev. Lett.* **1999**, *83*, 4880.

(25) Northrup, J. E. *Phys. Rev. B* **2007**, *76*, 245202.

(26) Cunningham, P. D.; Hayden, L. M. *J. Phys. Chem. C* **2008**, *112*, 7928.

(27) Day, J.; Platt, A. D.; Subramanian, S.; Anthony, J. E.; Ostroverkhova, O. *J. Appl. Phys.* **2009**, *105*, 103703.

(28) Xie, X.; Dai, J.; Zhang, X.-C. *Phys. Rev. Lett.* **2006**, *96*, 075005.

(29) Kress, M.; Loffler, T.; Eden, S.; Thomson, M.; Roskos, H. G. *Opt. Lett.* **2004**, *29*, 1120.

(30) Cook, D. J.; Hochstrasser, R. M. *Opt. Lett.* **2000**, *25*, 1210.

(31) Kim, K. Y.; Glownia, J. H.; Taylor, A. J.; Rodriguez, G. *Opt. Express* **2007**, *15*, 4577.

(32) Nienhuys, H. K.; Sundstrom, V. *Phys. Rev. B* **2005**, *71*, 235110.

(33) McCulloch, I.; Heeney, M.; Bailey, C.; Genevicius, K.; MacDonald, I.; Shkunov, M.; Sparrowe, D.; Tierney, S.; Wagner, R.; Zhang, W.; Chabinyc, M. L.; Kline, R. J.; McGehee, M. D.; Toney, M. F. *Nat. Mater.* **2006**, *5*, 328.

(34) Esenturk, O.; Kline, R. J.; Delongchamp, D. M.; Heilweil, E. J. *J. Phys. Chem. C* **2008**, *112*, 10587.

(35) Beard, M. C.; Blackburn, J. L.; Heben, M. J. *Nano Lett.* **2008**, *8*, 4238.

(36) Ai, X.; Beard, M. C.; Knutsen, K. P.; Shaheen, S. E.; Rumbles, G.; Ellingson, R. J. *J. Phys. Chem. B* **2006**, *110*, 25462.

(37) Ostroverkhova, O.; Cooke, D. G.; Shcherbyna, S.; Egerton, R.; Hegmann, F. A.; Tykwinski, R. R.; Anthony, J. E. *Phys. Rev. B* **2005**, *71*, 035204.

(38) Kline, R. J.; McGehee, M. D.; Kadnikova, E. N.; Liu, J.; Frechet, J. M. J.; Toney, M. F. *Macromolecules* **2005**, *38*, 3312.

(39) Anderson, P. W. *Phys. Rev.* **1958**, *109*, 1492.

(40) Smith, N. V. *Phys. Rev. B* **2001**, *64*, 155106.

(41) Turner, G. M.; Beard, M. C.; Schmuttenmaer, C. A. *J. Phys. Chem. B* **2002**, *106*, 11716.

(42) Cooke, D. G.; MacDonald, A. N.; Hryciw, A.; Wang, J.; Li, Q.; Meldrum, A.; Hegmann, F. A. *Phys. Rev.* **2006**, *73*, 193311.

(43) Walther, M.; Cooke, D. G.; Sherstan, C.; Hajar, M.; Freeman, M. R.; Hegmann, F. A. *Phys. Rev. B* **2007**, *76*, 125408.

(44) Dicker, G.; de Haas, M. P.; Warman, J. M.; de Leeuw, D. M.; Siebbeles, L. D. A. *J. Phys. Chem. B* **2004**, *108*, 17818.

(45) Hamadani, B. H.; Gundlach, D. J.; McCulloch, I.; Heeney, M. *Appl. Phys. Lett.* **2007**, *91*, 243512.

(46) Hendry, E.; Koeberg, M.; Schins, J. M.; Siebbeles, L. D. A.; Bonn, M. *Chem. Phys. Lett.* **2006**, *432*, 441.

(47) van der Horst, J.-W.; Bobbert, P. A.; de Jong, P. H. L.; Michels, M. A. J.; Siebbeles, L. D. A.; Warman, J. M.; Gelinck, G. H.; Brocks, G. *Chem. Phys. Lett.* **2001**, *334*, 303.

(48) Nemec, H.; Nienhuys, H. K.; Zhang, F.; Inganas, O.; Yartsev, A.; Sundstrom, V. *J. Phys. Chem. C* **2008**, *112*, 6558.

(49) Zheng, X.; McLaughlin, C. V.; Cunningham, P. D.; Hayden, L. M. *J. Nanoelectron. Optoelectron.* **2007**, *2*, 58.

(50) Liu, J.; Guo, X.; Dai, J.; Zhang, X.-C. *Appl. Phys. Lett.* **2008**, *93*, 171102.

JP906454G